Reaction Mechanism of Silicon−Hydrogen Bond Activation Studied Using Femtosecond to Nanosecond IR Spectroscopy and Ab Initio Methods

H. Yang,[†] M. C. Asplund,[§] K. T. Kotz,[†] M. J. Wilkens,[†] H. Frei,[‡] and C. B. Harris*[,†]

Contribution from the Department of Chemistry, University of California, Berkeley, California 94720, Chemical Sciences Division and Physical Biosciences Division, MS Calvin Laboratory, Ernest Orlando Lawrence Berkeley National Laboratory, Berkeley, California 94720

Received March 2, 1998

Abstract: The Si−H bond activation reactions by group VIIB, d^6 organometallic compounds η^5-$CpM(CO)_3$ (M = Mn, Re; Cp = C_5H_5) were studied in neat triethylsilane under ambient conditions. Utilizing femtosecond and nanosecond pump−probe spectroscopic methods, the spectral evolution of the CO stretching bands was monitored from 300 fs to tens of microseconds following UV photolysis. The reactive intermediates observed on the ultrafast time scale were also studied using ab initio quantum chemical modeling. It was found that photolysis of the manganese tricarbonyl resulted in dicarbonyls in their singlet or triplet electronic states, whereas photolysis of the rhenium complex led only to the singlet dicarbonyl. The branching ratio of the two manganese intermediates was measured and was related to different electronic excited states. For both the Mn and Re complexes, the reactions were found to be divided into two pathways of distinct time scales by the initial solvation of the dicarbonyls through the Si−H bond or an ethyl group of the solvent molecule. The time scale for the Si−H bond-breaking process was, for the first time, experimentally derived to be 4.4 ps, compared to 230 ns for breaking an alkane C−H bond. Knowledge of the elementary reaction steps including changes in molecular morphology and electronic multiplicity allowed a comprehensive description of the reaction mechanisms for these reactions.

I. Introduction

The photochemical oxidative addition of a Si−H bond to certain transition metal complexes has been the focus of many research efforts since its initial discovery.[1] This type of reaction, which cleaves, or activates, a Si−H bond, is critical in hydrosilation.[2,3] In addition, it provides a direct comparison to another important bond-cleavage reaction, C−H bond activation by similar transition metal complexes.[4] As such, knowledge of the reaction mechanism may facilitate the development of homogeneous catalysis[5] and lead ultimately to a general understanding of the chemistry of bond-cleavage reactions.

Many of the previous studies have used group VIIB, d^6 compounds η^5-$CpM(CO)_3$ (M = Mn, Re; Cp = C_5H_5) as model reagents. They provide an interesting contrast of reactivity in that the extent of the Si−H bond cleavage varies with the type of metal; the rhenium complex breaks the Si−H bond completely whereas there remains residual Si···H interaction in the manganese case.[6] Mechanistically, Young and Wrighton have established that, at low temperatures, the primary photochemical product upon UV irradiation of $CpMn(CO)_3$ is the coordinatively unsaturated, 16-e$^-$ $CpMn(CO)_2$ (Scheme 1a).[9] Further studies have shown that the resulting dicarbonyl is complexed by the solvent to form $CpMn(CO)_2$(solvent) and that the apparent rate-determining step involves a loosely solvated transition-state complex.[9−17] The reaction of the rhenium complex $CpRe(CO)_3$ with silanes (Scheme 1b) has also been found to begin with loss of a CO ligand, followed by solvent coordination. Despite the many experimental efforts in deriving the reaction mechanism, elementary reaction steps, including the early-time dynamics and the time scale of the Si−H bond-breaking step,

* To whom correspondence should be addressed.
† University of California and Chemical Sciences Division, LBNL.
‡ Physical Biosciences Division, MS Calvin Laboratory, LBNL.
§ Present address: Department of Chemistry, University of Pennsylvania.

(1) Jetz, W.; Graham, W. A. G. *Inorg. Chem.* **1971**, *10*, 4.
(2) Wrighton, M. S.; Schroeder, M. A. *J. Am. Chem. Soc.* **1974**, *96*, 6235.
(3) Schubert, U. *Adv. Organomet. Chem.* **1990**, *30*, 151.
(4) (a) Bromberg, S. E.; Yang, H.; Asplund, M. C.; Lian, T.; McNamara, B. K.; Kotz, K. T.; Yeston, J. S.; Wilkens, M.; Frei, H.; Bergman, R. G.; Harris, C. B. *Science* **1997**, *278*, 260. (b) Arndtsen, B. A.; Bergman, R. G.; Mobley, T. A.; Peterson, T. H. *Acc. Chem. Res.* **1995**, *28*, 154. (c) Bergman, R. G. *Science* **1984**, *223*, 902.
(5) (a) Masters, C. *Homogeneous Transition-metal Catalysis*; Chapman Hall: London, 1981. (b) Moser, W. R.; Slocum, D. W. *Homogeneous Transition Metal Catalyzed Reactions*; American Chemical Society: Washington, DC, 1992.
(6) For example, the distance between the silicon and the hydrogen atom in the adduct $CpRe(CO)_2(H)(SiPh_3)$ is 2.19 Å (Ph = phenyl, C_6H_5) (ref 7) compared to 1.80 Å for the similar Mn compound, $MeCpMn(CO)_2(H)(SiPh_2F)$ (MeCp = $CH_3C_5H_4$) (ref 8).
(7) Smith, R. A.; Bennett, M. J. *Acta Crystallogr., Sect. B* **1977**, *33*, 1113.
(8) (a) Schubert, U.; Ackermann, K.; Wörle, B. *J. Am. Chem. Soc.* **1982**, *104*, 7378. (b) Schubert, U.; Scholz, G.; Müller, J.; Ackermann, K.; Wörle, B.; Stansfield, R. F. D. *J. Organomet. Chem.* **1986**, *306*, 303.
(9) Young, K. M.; Wrighton, M. S. *Organometallics* **1989**, *8*, 1063.
(10) Hart-Davis, A. J.; Graham, W. A. G. *J. Am. Chem. Soc.* **1971**, *93*, 4388.
(11) Hill, R. H.; Wrighton, M. S. *Organometallics* **1987**, *6*, 632.
(12) Creaven, B. S.; Dixon, A. J.; Kelly, J. M.; Long, C.; Poliakoff, M. *Organometallics* **1987**, *6*, 2600.
(13) Klassen, J. K.; Selke, M.; Sorensen, A. A.; Yang, G. K. *J. Am. Chem. Soc.* **1990**, *112*, 1267.
(14) Burkey, T. J. *J. Am. Chem. Soc.* **1990**, *112*, 8329.
(15) Hester, D.; Sun, J.; Harper, A. W.; Yang, G. K. *J. Am. Chem. Soc.* **1992**, *114*, 5234.
(16) Hu, S.; Farrell, G. J.; Cook, C.; Johnston, R.; Burkey, T. J. *Organometallics* **1994**, *13*, 4127.
(17) Palmer, B. J.; Hill, R. H. *Can. J. Chem.* **1996**, *74*, 1959.

S0002-7863(98)00692-1 CCC: $15.00
Published on Web 09/22/1998

Scheme 1

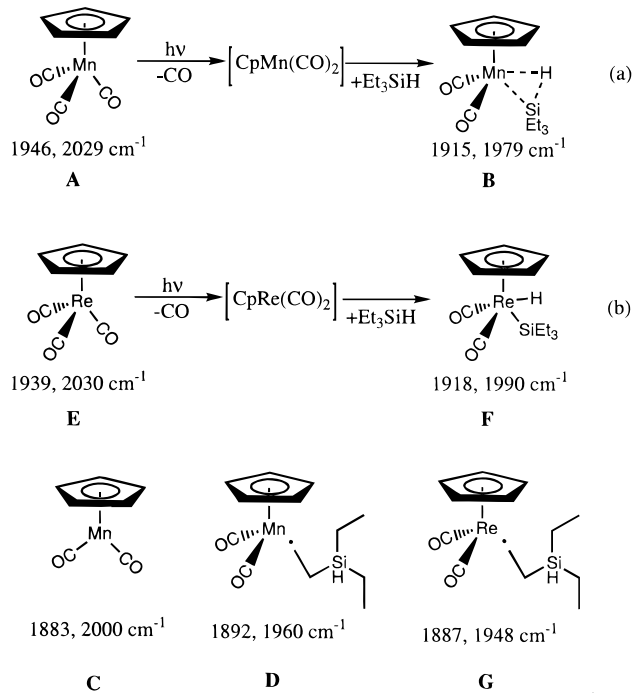

have remained unattainable due to the extremely rapid reaction rate.[16] Recently, our group has been able to investigate the room-temperature reaction dynamics of Si−H bond activation by $CpMn(CO)_3$ in neat Et_3SiH ($Et = C_2H_5$) using femtosecond infrared spectroscopy (ref 18, hereafter denoted as paper I). It was found that UV excitation of the parent compound $CpMn(CO)_3$ generated two dicarbonyls, and subsequent solvation partitioned the reaction into two parallel pathways.

In this article, we report the use of a combination of theoretical modeling and experimental measurements to continue pursuing this important reaction (Scheme 1). The elementary reaction steps from initial photolysis to completion of the reaction were studied to derive a comprehensive reaction mechanism. Due to the complexity of the reaction and for clarity, we summarize below some important findings of this work (cf. Figures 12 and 13) and leave the technicalities for later sections. The final results can be summarized as follows: (1) The early-time reaction dynamics depend critically on the electronic structure of the organometallic complex. For the manganese complex, there are two overlapping electronic bands in the accessible UV region (cf. Figure 10). The higher-energy band is related to formation of an unsolvated singlet dicarbonyl **D*** (an asterisk indicates excited state) and the lower one to triplet dicarbonyl **C**. A typical UV excitation of the parent molecule will populate both states, resulting in **C** or **D*** through *parallel* reaction channels. The branching ratios **A** → **C** → **D**:**A** → **D*** → **D** for these two parallel channels measured at 295- and 325-nm excitations are approximately 50%:50% and 75%:25%, respectively. For the rhenium complex, only one electronic band appears in the UV region; photolysis of the rhenium parent molecule leads exclusively to a singlet rhenium dicarbonyl, **G***. (2) For both metal complexes, initial solvation of the nascent coordinatively unsaturated dicarbonyls (**C**, **D***, and **G***), via either the ethyl moiety or the Si−H bond of the solvent molecule Et_3SiH, partitions the reaction into two pathways. Solvation of the metal dicarbonyl through the Si−H bond leads directly to the final products **B** or **F** on the ultrafast time scale. Solvation through an ethyl group results in reactive intermediate **D** or **G**, which reacts further to form the final products in 177 ns and 6.8 μs, respectively. (3) The relative probabilities of (solvation through the ethyl moiety):(solvation through the Si−H bond) for the Mn and Re complexes are 5.3 and 3, respectively. The differences are attributed to steric effects. The larger diameter of the rhenium atom allows equivalent sampling of the chemically different sites in a solvent molecule (three ethyl groups and one Si−H bond). (4) The apparent rate-determining step for both reactions is the dissociative rearrangement from the ethyl solvates **D** or **G** to the final products. The corresponding free-energy barriers for the manganese and rhenium complexes, determined from simple transition-state theory, are 8.25 ± 0.03 and 10.41 ± 0.02 kcal/mol, respectively. (5) The time scale for a Si−H bond-breaking process is, for the first time, estimated to be 4.4 ± 2.6 ps, indicative of a low-barrier, if any, reaction.

The paper is organized as follows: The experimental methods and calculation procedures are described in section II. The results and detailed data analysis are presented in section III, in the order of manganese/experimental, rhenium/experimental, and theoretical results. Implications of the results are discussed in section IV. In particular, for the manganese complex, we discuss the effects of sampling different regions of electronically excited potential energy surface, the nature of the observed transient intermediates, and their interaction with solvent. Comprehensive reaction mechanisms are described in the end of section IV-A for Mn and in section IV-B for Re. Finally, current results are compared to the C−H bond activation in section V.

II. Methods

Sample Handling. The compounds η^5-$CpMn(CO)_3$ (99%, **A**) and η^5-$CpRe(CO)_3$ (99%, **E**) were purchased from Strem, Inc. and used without further purification. To ensure that moisture and oxygen did not interfere with the experiment, the triethylsilane acquired from Gelest, Inc. was dried in an alumina column and distilled under nitrogen. The sample was prepared under nitrogen atmosphere in an airtight, demountable liquid IR flow cell (Harrick Scientific Corp.). The concentration of the $CpMn(CO)_3/Et_3SiH$ solution was approximately 25 mM. The absorbance of a 400-μm-thick sample of this concentration at 325 nm was about 1 OD. The concentration of the $CpRe(CO)_3/Et_3SiH$ solution was approximately 9 mM, to give ~0.6 OD absorbance at 295 nm with a 630-μm-thick cell. During the course of experiment, the static IR spectra were checked regularly to monitor sample degradation.

Femtosecond Infrared Spectroscopy. Details of the femtosecond IR (fs-IR) spectrometer setup have been published elsewhere.[19] In brief, the output of a Ti:sapphire oscillator was amplified in two prism-bored dye-cell amplifiers,[20] which were pumped by the output of a frequency-doubled 30-Hz Nd:YAG laser. The amplified light, centered at ~810 nm, was then split into three beams. One beam was further amplified to give 70-fs, 20-μJ pulses. The other two beams were focused into two sapphire windows to generate a white light continuum. Desired wavelengths of the white light were selected by two band-pass (BP) filters whose full widths at half-maximum (fwhm) were 10 nm and further amplified by three-stage dye amplifiers. In this study, the excitation pulses of 295 and 325 nm were generated by respectively frequency doubling 590- and 650-nm light. The resulting UV photons (with energy of ~6 μJ/pulse) were focused into a disk of ~200 μm diameter at the sample to initiate chemical reactions. The required time delay between a pump pulse and a probe pulse was achieved by guiding the 590-nm beam (or the 650-nm beam) through a variable delay line before it was frequency doubled.

(18) Yang, H.; Kotz, K. T.; Asplund, M. C.; Harris, C. B. *J. Am. Chem. Soc.* **1997**, *119*, 9564.

(19) Lian, T.; Bromberg, S. E.; Asplund, M. C.; Yang, H.; Harris, C. B. *J. Phys. Chem.* **1996**, *100*, 11994.

(20) Bethune, D. S. *Appl. Opt.* **1981**, *20*, 1987.

The broad-band, ultrafast probe pulses centered at ~5 μm were generated by mixing a 690-nm with an 810-nm beam. The resulting ~1-μJ IR pulses, having temporal fwhm of about 70 fs and spectral bandwidth of about 200 cm^{-1}, were split into signal and reference beams. Both the signal beam and the reference beam were then focused into a monochromator and received by a pair of HgCdTe detectors. The time-resolved IR spectra were collected by scanning the monochromator while fixing the time delay between the pump and the probe pulses. The kinetic traces were acquired by setting the monochromator at the desired wavelengths while varying the delay between pump and probe. The typical spectral and temporal resolutions for this setup are 4 cm^{-1} and 300 fs, respectively. The polarizations of the pump and the probe pulse were set at the magic angle (54.7°) to ensure that all signals were due to population dynamics. A broad, wavelength-independent background signal from CaF_2 windows when pumping at 295 nm has been subtracted from the transient spectra and kinetic traces.

Nanosecond Step-Scan FTIR. These measurements were made using a step-scan FTIR spectrometer described elsewhere.[21] The instrument is based on a Bruker IFS-88 FTIR with a special scanner module to allow step-scanning. An InSb detector with a 40-ns fwhm measured from the IR scatter of 1064-nm light from a YAG laser was used. The IR light was focused in the cavity with two 10-mm-focal length BaF_2 lenses, which gave beam sizes smaller than those given by comparable curved mirrors, allowing increased IR throughput and less sample degradation. The sample was photoexcited with 10-ns pulses from either the fourth harmonic output of a YAG laser or the second harmonic of a dye laser tuned to 590 nm.

Quantum Chemical Modeling. First-principle methods provide a means by which to study the nature of possible candidates for the observed reactive intermediates whose lifetimes are too short for conventional characterization. To represent the intermediates in a practically tractable way, the complexation of the ethyl moiety of Et_3SiH with the metal fragment η^5-$CpM(CO)_2$ was modeled by the complexation of an ethane molecule with η^5-$CpM(CO)_2$. The final products, η^5-$CpM(CO)_2(H)(SiEt_3)$, were modeled by η^5-$CpM(CO)_2(H)(SiH_2CH_3)$. The standard lanl2dz basis set was employed throughout the calculations.[22] This basis set uses a nonrelativistic effective core potential (ECP) for Mn and a relativistic one for Re. The geometries for metal complexes in the singlet state were optimized at the second-order Møller−Plesset perturbation theory (MP2) level. Those of the triplet state were optimized at the unrestricted MP2 (UMP2) level of theory. During the optimization, no constraints other than that of a 180° M−C−O bond angle were imposed. These MP2 calculations were carried out using the GAUSSIAN-92 package.[23,24]

UMP2 calculations have been known to tend to give incorrect energies for the triplet electronic states due to contamination from other electronic states of higher spin multiplicity, especially when there is near-degeneracy.[25] Therefore, calculations on the 16-e^- species using density functional theory (DFT) at the B3LYP/lanl2dz level were also carried out to verify the MP2 results. The Gaussian92/DFT package was used for the DFT calculations.[26] To minimize the near-degeneracy effect on the calculated energy, the complete active space multiconfigurational self-consistent field (CAS-MCSCF) followed by second-order many-particle perturbation treatment (PT2) were carried out at the DFT geometries. Again, the lanl2dz basis set[22,27] was used in the CAS-MCSCF-PT2 calculations. The restricted open-shell Hartree−Fock (ROHF) wave functions were calculated as the starting orbitals for subsequent CAS-MCSCF calculations. During the CAS-MCSCF calculations, the five d-orbitals and the corresponding five d-type virtual orbitals were correlated. The resultant CAS-MCSCF wave functions were then used for the second-order perturbation method of Nakano implemented into GAMESS-US.[28,29]

The metal−ligand interaction energies were calculated as the energy difference between the products and the reactant in the reaction,

$$CpM(CO)_2L \rightarrow CpM(CO)_2 + L \qquad (1)$$

where L could be CO, H_3CCH_3, or $HSiH_2CH_3$. The basis set superposition error (BSSE)[30] correction was calculated using a fragment relaxation procedure recently proposed by Xantheas,[31] which gives correct results at the complete basis set limit:

$$\Delta E = E_{ZL}^{\alpha\cup\beta}(ZL) - E_{Z}^{\alpha}(Z) - E_{L}^{\beta}(L) + E_{rel}^{\alpha}(Z) + E_{rel}^{\beta}(L) \qquad (2)$$

where

$$E_{rel}^{\alpha}(Z) = E_{ZL}^{\alpha}(Z) - E_{Z}^{\alpha}(Z)$$
$$E_{rel}^{\beta}(L) = E_{ZL}^{\beta}(L) - E_{L}^{\beta}(L) \qquad (3)$$

In the above equations, Z represents the metal fragment $CpM(CO)_2$ and L the ligands, the constituent basis sets of which are denoted α and β, respectively. Except for the ethane complex, the zero point energy (ZPE) correction to the complexation energy was calculated numerically from vibrational frequencies at the Hartree−Fock level. Because of the weak interaction between an alkane molecule and a transition metal, the ZPE correction to the metal−alkane interaction energy has been found to be typically smaller than 1 kcal/mol. Our MP2 frequency calculations on the ZPE correction for the η^5-$CpMn(CO)_2(H_3CCH_3)$ complexation reaction gave a 0.21 kcal/mol ZPE correction. In our calculations, the same 0.21 kcal/mol ZPE correction was used on both the Mn and the Re alkane complexes.

III. Results

The infrared spectra in the CO stretching region are presented in a form of difference absorbance in which positive bands indicate the appearance of new species while negative bands (bleaches) represent the depletion of parent molecules. In the ultrafast spectra of each metal complex, the bottom panel is an FTIR difference spectrum of the sample taken a few minutes after prolonged exposure to 308-nm UV pulses from an excimer laser.

A. Activation of the Silicon−Hydrogen Bond of Et_3SiH by $CpMn(CO)_3$. Shown in Figure 1 are the fs-IR spectra of η^5-$CpMn(CO)_3$ in neat Et_3SiH following excitation at 325 nm.

(21) Sun, H.; Frei, H. *J. Phys. Chem. B* **1997**, *101* 205.

(22) (a) Dunning, T. H., Jr.; Hay, P. J. In *Methods of Electronic Structure Theory*, Schaefer, H. F., III, Ed.; Plenum: New York, 1977; Vol. 2. (b) Hay, P. J.; Wadt, W. R. *J. Chem. Phys.* **1985**, *82*, 270. (c) Hay, P. J.; Wadt, W. R. *J. Chem. Phys.* **1985**, *82*, 284. (d) Hay, P. J.; Wadt, W. R. *J. Chem. Phys.* **1985**, *82*, 299.

(23) Frisch, M. J.; Trucks, G. W.; Head-Gordon, M.; Gill, P. M. W.; Wong, M. W.; Foresman, J. B.; Johnson, B. G.; Schlegel, H. B.; Robb, M. A.; Replogle, E. S.; Gomperts, R.; Andres, J. L.; Raghavachari, K.; Binkley, J. S.; Gonzalez, C.; Martin, R. L.; Fox, D. J.; Defrees, D. J.; Baker, J.; Stewart, J. J. P.; Pople, J. A. *Gaussian 92, Revision E.2*; Gaussian: Pittsburgh, PA, 1992.

(24) Calculations were performed on workstations in our laboratory and those at the Molecular Graphics Facility of the College of Chemistry, University of California at Berkeley.

(25) Schlegel, H. B. *J. Chem. Phys.* **1986**, *84* 4530.

(26) Frisch, M. J.; Trucks, G. W.; Schlegel, H. B.; Gill, P. M. W.; Johnson, B. G.; Wong, M. W.; Foresman, J. B.; Robb, M. A.; Head-Gordon, M.; Replogle, E. S.; Gomperts, R.; Andres, J. L.; Raghavachari, K.; Binkley, J. S.; Gonzalez, C.; Martin, R. L.; Fox, D. J.; Defrees, D. J.; Baker, J.; Stewart, J. J. P.; Pople, J. A. *Gaussian 92/DFT, Revision G.1*; Gaussian: Pittsburgh, PA, 1993.

(27) Basis sets were obtained from the Extensible Computational Chemistry Environment Basis Set Database, Version 1.0, as developed and distributed by the Molecular Science Computing Facility, Environmental and Molecular Sciences Laboratory, which is part of the Pacific Northwest Laboratory, P.O. Box 999, Richland, WA 99352, and funded by the U.S. Department of Energy. The Pacific Northwest Laboratory is a multiprogram laboratory operated by Battelle Memorial Institute for the U.S. Department of Energy under Contract DE-AC06-76RLO 1830. Contact David Feller, Karen Schuchardt, or Don Jones for further information.

(28) (a) Nakano, H. *J. Chem. Phys.* **1993** *99*, 7983−7992. (b) Nakano, H. *Chem. Phys. Lett.* **1993** *207*, 372−378.

(29) Schmidt, M. W.; Baldridge, K. K.; Boatz, J. A.; Elbert, S. T.; Gordon, M. S.; Jensen, J. H.; Koseki, S.; Matsunaga, N.; Nguyen, K. A.; Su, S. J.; Windus, T. L.; Dupuis, M.; Montgomery, J. A. *J. Comput. Chem.* **1993**, *14*, 1347−1363.

(30) Liu, B.; McLean, A. D. *J. Chem. Phys.* **1973**, *59*, 4557.

(31) Xantheas, S. S. *J. Chem. Phys.* **1996**, *21*, 8821.

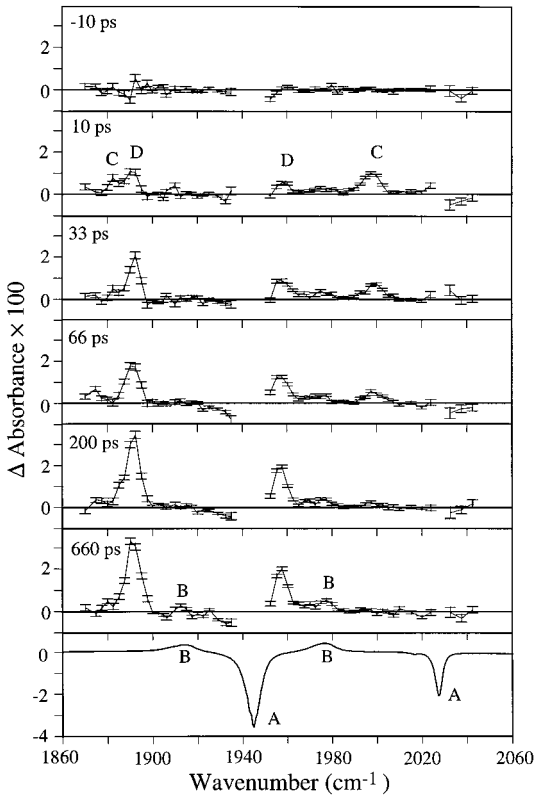

Figure 1. Transient difference spectra in the CO stretching region for $CpMn(CO)_3$ in neat triethylsilane at −10, 10, 33, 66, 200, and 660 ps following 325-nm UV photolysis. Under the experimental conditions, the large cross section of the solvent Si−H band (∼2100 cm^{-1}) and the parent CO bands (1947 and 2028 cm^{-1}) make it difficult to access some regions of the spectrum (ref 32). The last panel is an FTIR difference spectrum before and after UV photolysis at 308 nm.

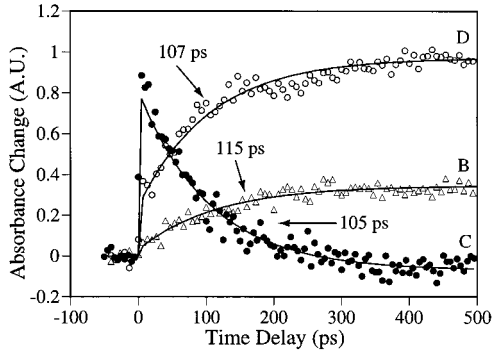

Figure 2. Ultrafast kinetics of $CpMn(CO)_3$ in neat triethylsilane after 325-nm UV photolysis at (B) 1979 cm^{-1}, the CO stretch of the silyl adduct $CpMn(CO)_2(H)(SiEt_3)$ (△); (C) 2002 cm^{-1} (●); and (D) 1892 cm^{-1} (○). The wavelengths were chosen to minimize overlap with adjacent peaks. The time constants for the exponential fits (dashed lines) are shown in the graph.

The peaks at 1892 and 1960 cm^{-1} are assigned to η^5-$CpMn(CO)_2(Et_3SiH)$, denoted **D** (Scheme 1). Having also been observed in low-temperature studies,[11,16] **D** is attributed to solvation of η^5-$CpMn(CO)_2$ through the ethyl moiety of Et_3-SiH. In the 10-ps panel of Figure 1, the two bands at ∼2000 and ∼1883 cm^{-1}, which disappear at longer time scales, are attributed to a triplet dicarbonyl species, denoted **C** (see section IV for assignment). Figure 2 shows the kinetic traces of **D**, **C**, and the final product **B** following 325-nm excitation. The kinetics of **C** recorded at 2000 cm^{-1} exhibit a rapid rise and an 105 ± 8.0 ps decay.[33] The product band at 1979 cm^{-1} displays a single-exponential rise of 115 ± 14 ps.

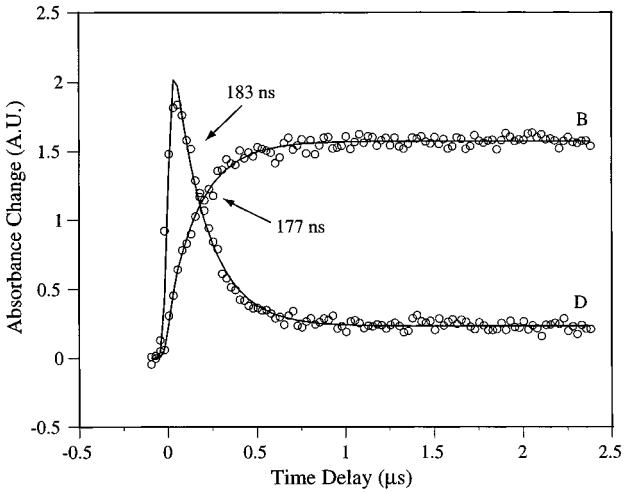

Figure 3. Nanosecond kinetics (○) of $CpMn(CO)_3$ in neat triethylsilane after 295-nm UV photolysis at (B) 1979 cm^{-1}, the CO stretch of the silyl adduct $CpMn(CO)_2(H)(SiEt_3)$ and (D) 1892 cm^{-1}. The finite intensity of the 1892-cm^{-1} kinetic trace at longer delay time is probably due to $CpMn(^{13}CO)(^{12}CO)(H)(SiEt_3)$ which has a CO absorption at ∼1887 cm^{-1}.[37] The time constants for the exponential fits (dashed lines) are shown in the graph.

The kinetic trace of **D** at 1892 cm^{-1} exhibits a fast rise and then gradually grows to a constant level. It can be described by the equation,

$$\text{signal}(t) = C_1(1 - e^{-t/\tau}) + C_2 \qquad (4)$$

where τ is a formation time constant, and C_1 and C_2 are amplitude constants. This same equation will be used later in modeling kinetic traces of similar behavior. The fitted numeric values for τ, C_1, and C_2 are 107 ± 8.9 ps, 0.73 ± 0.033, and 0.25 ± 0.033, respectively. Clearly, the decay of the intermediate **C** is correlated to the formation of both the ethyl solvate **D** and the final product **B**. Equation 4 implies two channels for the formation of the ethyl solvate η^5-$CpMn(CO)_2(Et_3SiH)$, the branching ratio of which is represented by the relative magnitude of C_1 to C_2. With a typical solvation time of a few picoseconds in mind, the channel that contributes to the fast rise C_2 of the transient of **D** is attributed to solvation of a singlet η^5-$CpMn(CO)_2$, denoted **D***. The other channel that contributes to the 107-ps rise is attributed to interconversion from **C**. Consequently, the branching ratio of the reaction pathway **A** → **C** → **D** to the pathway **A** → **D*** → **D** in this case is approximately 3:1. The implications of these results will be discussed in section IV.

The long-time behavior of the reaction was studied using a nanosecond step-scan FTIR spectrometer. Displayed in Figure 3 are the kinetics of **D** and that of the product **B**, recorded at 1892 and 1979 cm^{-1}, respectively. **D** shows an instrument-limited rise and then decays with a time constant of 183 ± 8

(32) The extinction coefficients ϵ for ν (CO) of $CpMn(CO)_3$ are 12 700 M^{-1} cm^{-1} and 5700 M^{-1} cm^{-1} for the 1947- and 2028-cm^{-1} peaks, respectively (ref 11). To prepare a sample which has an OD ≈ 1 at the pump wavelength of 325 nm, the IR absorbances of the 1947- and 2028-cm^{-1} bands are calculated to be 12.7 and 5.7, respectively (25 mM, 500-μm cell). Similarly, to prepare a sample which has an OD ≈ 0.6 at the pump wavelength of 295 nm, the IR absorbances of the 1939- and 2030-cm^{-1} bands are calculated to be 9.2 and 3.3 OD, respectively (9 mM, 630-μm cell). A thinner cell was used to acquire kinetics for the parent molecule. Such an experimental difficulty is expected when the sample has a low absorption cross section in the UV but a high extinction coefficient in the probe IR region. A sample calculation to estimate the signal strength is included in ref 36.

(33) Uncertainties represent one standard deviation.

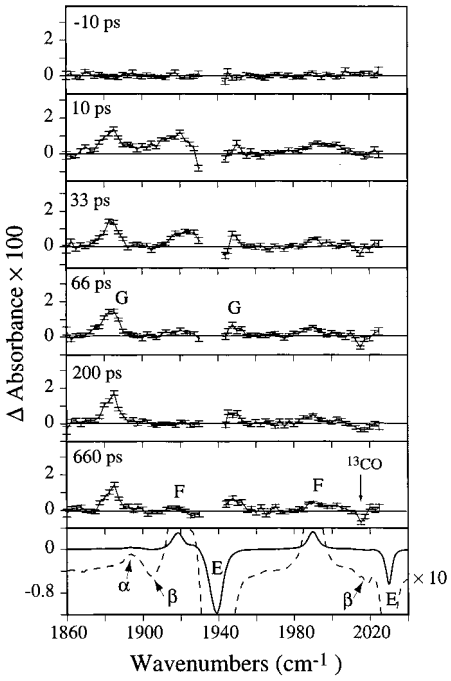

Figure 4. Transient difference spectra in the CO stretching region for $CpRe(CO)_3$ in neat triethylsilane at −10, 10, 33, 66, 200, and 660 ps following 295-nm UV photolysis. The arrow at ∼2015 cm^{-1} indicates the bleach due to photolysis of the naturally abundant $CpRe(^{12}CO)_2(^{13}CO)$.[36] Last panel: An FTIR difference spectrum before and after UV photolysis at 308 nm. Enlarged spectrum (10× and offset by −0.49) is displayed as a dashed line to show (α) a peak of $CpRe(^{13}CO)(^{12}CO)(H)(SiEt_3)$ at ∼1892 cm^{-1}; and (β) bleaches of $CpRe(^{13}CO)(^{12}CO)_2$ at ∼1906 and ∼2019 cm^{-1}.

ns. **B** exhibits a fast rise and an exponential growth of 177 ± 7 ns. The rapid rise of **B** is from the remnant of the initial Si−H solvate that forms in the ultrafast time scale. As has been discussed in paper I, the latter exponential rise of **B** is due to the dissociative rearrangement from **D**.[18,34] The nanosecond kinetics of **B** can also be modeled with eq 4. In this case, the coefficients C_1 and C_2 represent the relative probability of initial solvation through the ethyl moiety (84%) or the Si−H bond (16%), respectively. These numbers, however, should be treated in a qualitative manner. The greater excitation photon flux in our nanosecond setup compared to the femtosecond one may cause a transient temperature increase in the sample, which in turn may result in a time-dependent change in the index of refraction.[35] Such a thermal effect makes it difficult to quantify the observed kinetics rigorously.

Finally, the free-energy barrier of the dissociative process from **D** to **B** can be derived from the kinetic traces. If one assumes a simple transition-state theory, the reaction rate can be expressed as the reciprocal of the observed lifetime τ,

$$\text{reaction rate} \approx \frac{1}{\tau} = \frac{k_B T}{h} e^{-\Delta G^{\ddagger}/k_B T} \qquad (5)$$

where k_B is the Boltzmann constant, h Plank's constant, T room temperature (298.15 K), and $\Delta G^{\ddagger}$ the free energy of activation. The reaction barrier, estimated from the product formation time, is $\Delta G^{\ddagger} = 8.25 \pm 0.03$ kcal/mol. This is in excellent agreement with the literature value, 8.56 ± 0.49 kcal/mol, which is extrapolated to room temperature using the activation parameters obtained from low-temperature measurements.[11]

B. Activation of the Silicon−Hydrogen Bond of Et_3SiH by $CpRe(CO)_3$. Displayed in Figure 4 are the transient fs-IR spectra of $CpRe(CO)_3$ in neat Et_3SiH following excitation at 295 nm. The bottom panel is an FTIR difference spectrum taken after prolonged exposure to 308-nm light. The presence of naturally abundant ^{13}CO stretches is evidenced by the enlarged FTIR spectrum.[36] The small peak at 1892 cm^{-1} is assigned to η^5-$CpRe(^{13}CO)(^{12}CO)(H)(SiEt_3)$, denoted α in the enlarged spectrum. The shallow bleaches labeled as β are due to depletion of naturally abundant η^5-$CpRe(^{12}CO)_2(^{13}CO)$.[37] At the 10-ps panel, the pair of bands at 1887 and 1948 cm^{-1} are assigned to η^5-$CpRe(CO)_2(Et_3SiH)$ [**G**], resulting from solvation of the η^5-$CpRe(CO)_2$ [**G***] through the ethyl moiety of the solvent.[11] The final product **F** appears as two bands at 1918 and 1990 cm^{-1}, but its early-time spectra are complicated by absorptions from vibrationally excited parent molecules **E** (the 10- and 33-ps panels).

As shown in Figure 5a, the kinetics of the parent molecule **E** taken at 2030 cm^{-1} display an instrument-limited depletion which recovers with a time constant of 39.3 ± 1.6 ps to 28% of its initial intensity, consistent with the literature quantum yields of 0.30 at 313-nm excitation.[38] The recovery of the parent bleach is attributed to reestablishing the thermal distribution of vibrational states in the electronic-ground manifold.[39−41,43]

(34) For a recent discussion on the "chain-walk" mechanism vs the "dissociative" mechanism, see: Ladogana, S.; Nayak, S. K.; Smit, J. P.; Dobson, G. R. *Inorg. Chem.* **1997**, *36*, 650.

(35) Yuzawa, T.; Kato, C.; George, M. W.; Hamaguchi, H.-O. *Appl. Spectrosc.* **1994**, *48*, 684.

(36) In the following, we will use the Re system as an example to estimate the signal size of **F** in the ultrafast spectra. The same calculation is applicable to Mn spectra. We start by calculating the OD change in one of the parent bands, e.g., the 2030-cm^{-1} band. The pump beam consists of 295-nm pulses of energy ∼6 μJ, 75% of which are absorbed by an OD ≈ 0.6 sample. Change in the parent absorbance is calculated by $\Delta OD(E) = \epsilon l \Delta c_{parent}$, where l is the sample cell thickness and Δc_{parent} is the concentration change of the parent species in the cylindric volume defined by the pump beam. Taking into account the cell thickness (650 μm), the beam size at the sample (∼200 μm), and quantum yield (∼0.3), each pump pulse induces OD change in the parent bleach of ∼0.06. The signal size of **F** on the ultrafast time scale can be expressed as

$$\Delta OD(\mathbf{F}) = \Delta OD(\mathbf{E}) \times X(\mathbf{F}) \times \frac{\epsilon(\mathbf{F})}{\epsilon(\mathbf{E})}$$

where $X(\mathbf{F}) = 0.248 \pm 0.079$ is the branching percentage for **F** measured from the nanosecond kinetics, and the extinction coefficient ratio $\epsilon(\mathbf{F})/\epsilon(\mathbf{E}) \approx 2/5$ measured from the static difference FTIR spectrum on the bottom panel of Figure 1. $\Delta OD(\mathbf{F})$ is thus calculated to be ∼0.006, which is consistent with what we have measured in the present work. The above calculation also serves as a cross-examination for the measured 25% branching ratio in the initial solvation through the Si−H bond of Et_3SiH. The recorded ^{13}C bleach signal in the ultrafast spectra of the Re complex may appear somewhat larger than one would have expected from a simple estimate. In the following, we show that the Re spectra displayed reasonable ^{13}C bleach at 2015 cm^{-1}. Take the 200 ps panel of Figure 4 as an example. The numerical values for the 1990-cm^{-1} band of **F** and the ^{13}C bleach at 2015 cm^{-1} are about 0.0053 ± 0.0005 OD and −0.0036 ± 0.001 OD, respectively. Assuming 3% natural abundance of ^{13}C, and taking into account the difference in extinction coefficients $\epsilon(\mathbf{F})/\epsilon(^{13}C) \approx 2/5$ and branching ratios 0.248 ± 0.079, one finds that the estimated signal size of the ^{13}C bleach is ∼ −0.0017 ± 0.0005 OD, within a 95% confidence interval compared to recorded signal size (−0.0036 ± 0.001 OD). Similarly, the corresponding ^{13}C bleach of Mn complex has a signal size of −0.0027 ± 0.0006 OD (taken from the 660-ps panel of Figure 1), which is also reasonable within experimental error.

(37) CO frequencies of $CpRe(^{13}CO)_x(^{12}CO)_{3-x}$ in room-temperature alkane solutions were estimated from an effective force field calculation following the methods in: (a) Haas, H.; Sheline, R. K. *J. Chem. Phys.* **1967**, *47*, 2996. (b) Wilson, E. B., Jr.; Decius, J. C.; Cross, P. C. *Molecular Vibrations*; Dover: New York, 1980. The calculated frequencies (in cm^{-1}) are $CpRe(^{12}CO)_3$ [1939, 2030]; $CpRe(^{12}CO)_2(^{13}CO)$ [1906, 1939, 2019]; $CpRe(^{12}CO)(^{13}CO)_2$ [1895, 1919, 2005]; and $CpRe(^{13}CO)_3$ [1895, 1985]. Similarly, peaks originating from $CpM(^{13}CO)(^{12}CO)(H)(SiEt_3)$ are also estimated to be at 1892 and 1974 cm^{-1} for the rhenium complex and at 1887 and 1964 cm^{-1} for the manganese complex.

(38) Giodano, P. J.; Wrighton, M. S. *Inorg. Chem.* **1976**, *16*, 160.

(39) King, J. C.; Zhang, J. Z.; Schwartz, B. J.; Harris, C. B. *J. Chem. Phys.* **1993**, *99*, 7595 and references therein.

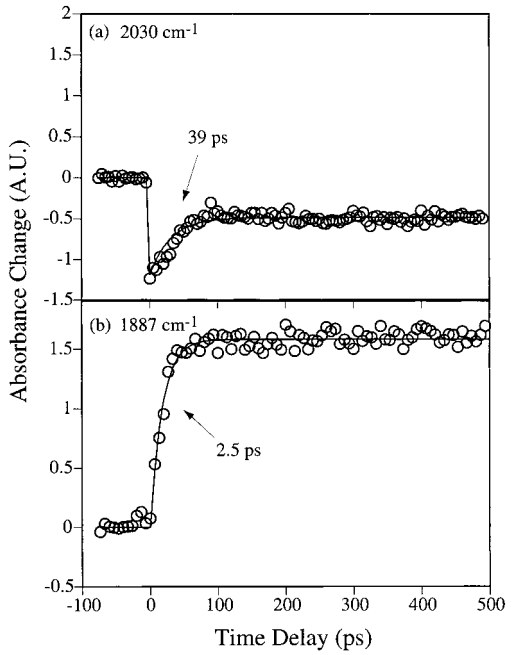

Figure 5. Ultrafast kinetics (○) of $CpRe(CO)_3$ in neat triethylsilane after 295-nm UV photolysis at (a) 2030 cm^{-1}, (the A-band of the CO stretches of the parent molecule; 100-μm cell was used to record this kinetic trace) and (b) 1887 cm^{-1}. The time constants obtained from exponential fits (solid lines) to the kinetic traces are also shown in the graph.

Processes that contribute to this nonequilibrated vibrational distribution include depletion of the $v = 0$ state by the pump photon and population replenished by nondissociative processes. As a consequence of populating the higher vibrational states, transitions such as $v = 1 \rightarrow 2$ and $v = 2 \rightarrow 3$ would become detectable. The broad band at ~1921 cm^{-1} is assigned to the $v = 1 \rightarrow 2$ absorption of the 1939-cm^{-1} CO stretching band of **E**, which evolves to the blue end of the spectrum and decays completely at later time (10-ps panel, Figure 4). The observed ~18-cm^{-1} anharmonicity is consistent with the reported anharmonicity of other metal carbonyls.[40−43] Similarly, the broad bands at ~2004 and ~1990 cm^{-1} in the 10-ps panel of Figure 4 can be assigned to the $v = 1 \rightarrow 2$ and $v = 2 \rightarrow 3$ absorption of naturally abundant $CpRe(^{13}CO)(CO)_2$, respectively. The parent molecules, containing one ^{13}CO ligand, manifest themselves as a depletion at 2015 cm^{-1}, as indicated by the arrow in the 660-ps panel of Figure 4 [see ref 37 for estimation of CO stretching frequencies of $CpRe(^{13}CO)_x(^{12}CO)_{3-x}$]. Unfortunately, this 2015-cm^{-1} band is superimposed on one of the parent $CpRe(^{12}CO)_3$ $v = 1 \rightarrow 2$ transition. Therefore, instead of showing an instantaneous depletion followed by a rapid recovery, it bleaches gradually to a constant level (Figure 6c).

The vibrationally hot bands described above unavoidably impede an accurate description of bands that are important in determining the reaction dynamics. The 1990-cm^{-1} band of the final product **F** overlaps with the $v = 2$ hot band (at ~1900 cm^{-1}) of the $CpRe(^{13}CO)(CO)_2$ bleach at 2015 cm^{-1}. As a result, the kinetic trace of **F** measured at 1990 cm^{-1} exhibits a sharp rise due to the hot band and then decays to a constant level (Figure 6). To derive the underlying product dynamics,

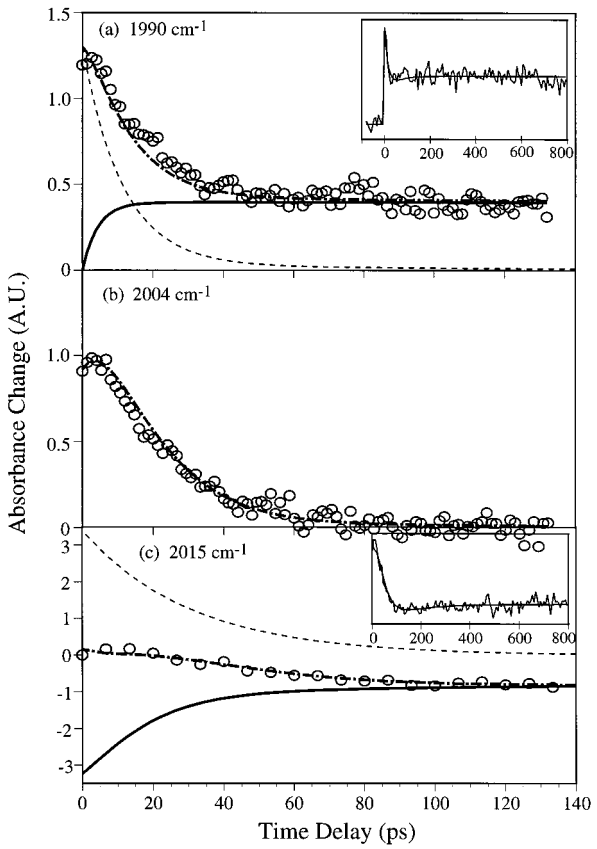

Figure 6. Modeling of the observed transient traces of $CpRe(CO)_3$ (cf. Appendix). (a) The transient trace recorded at the 1990-cm^{-1} product band (○). The solid line is the deconvolved product formation kinetics and the dashed line is the contribution from vibrationally excited $CpRe(^{12}CO)_2(^{13}CO)$. The observed kinetic trace is obtained (the dash−dot line) by reconvolving these two traces. Inset: A long scan at the same wavelength, showing that the amplitude of this peak remains the same up to ~1 ns. (b) The transient trace (○) of the 2005-cm^{-1} band, which is attributed to vibrationally excited $CpRe(^{12}CO)_2(^{13}CO)$. The dash−dot line follows the model presented in the Appendix. (c) The transient trace recorded at the 2015-cm^{-1} parent bleach (○) due to photolysis of the naturally abundant $CpRe(^{12}CO)_2(^{13}CO)$. The solid line is the deconvolved bleach recovery, and the dashed line is the reconstructed kinetics from the vibrationally excited $CpRe(^{12}CO)_3$.

the kinetic traces measured at 1990, 2004, and 2015 cm^{-1} were fit to a model which takes into account the bleach recovery, product formation, and vibrational relaxation (see Appendix). The extracted formation time for the product is 4.4 ± 2.6 ps. Typically, the initial solvation of metal carbonyls occurs within 1−2 ps following photolysis of one CO ligand,[39] from which one can infer the time scale for a barrierless associative reaction in solution. Accordingly, our results suggest that solvation of the η^5-$CpRe(CO)_2$ through the Si−H bond of the solvent leads directly to the formation of the product.

The kinetics of **G** measured at 1887 cm^{-1} show an exponential rise of 2.5 ± 1.6 ps and remain at the same intensity to ~1 ns (Figure 5b). As indicated by the absence of peaks at 1887 and 1948 cm^{-1} in the static FTIR spectrum at the bottom panel of Figure 4, this alkyl solvate must eventually react further to form the final product. To investigate the long-time behavior of this chemical system, we also performed nanosecond step-scan FTIR experiments. Representative kinetics of the alkyl solvate (**G**) and the product (**F**) are shown in Figure 7. The kinetics of the product **F** measured at 1990 cm^{-1} show an instrument-limited rise and an exponential growth of 6.8 ± 0.2 μs. The alkyl solvate recorded at 1887 cm^{-1} shows a 7.2 ±

(40) Lian, T.; Bromberg, S. E.; Yang, H.; Proulx, G.; Bergman, R. G.; Harris, C. B. *J. Am. Chem. Soc.* **1996**, *118*, 3769.
(41) Dougherty, T. P.; Grubbs, W. T.; Heilweil, E. J. *J. Phys. Chem.* **1994**, *98*, 9396.
(42) Arrivo, S. M.; Dougherty, T. P.; Grubbs, W. Y.; Heilweil, E. J. *Chem. Phys. Lett.* **1995**, *235*, 247.
(43) Dougherty, T. P.; Heilweil, E. J. *J. Chem. Phys.* **1994**, *100*, 4006.

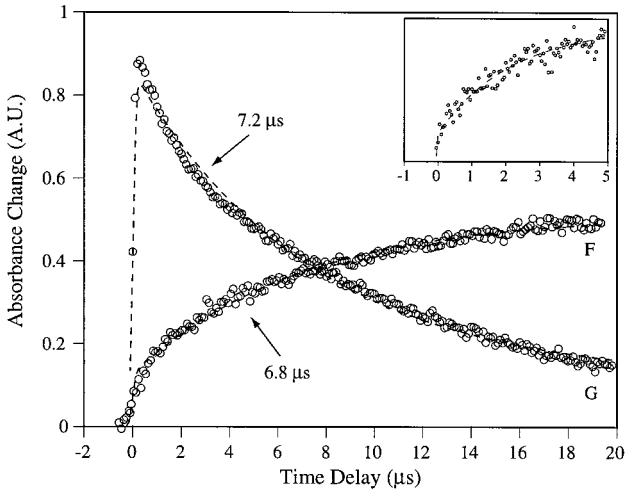

Figure 7. Nanosecond kinetics (○) of $CpRe(CO)_3$ in neat triethylsilane after 295-nm UV photolysis at (F) 1990 cm^{-1}, the CO stretch of the silyl adduct $CpRe(CO)_2(H)(SiEt_3)$, and (G) 1950 cm^{-1}, the CO stretch of the alkyl solvate $CpRe(CO)_2(Et_3SiH)$. The time constants for the exponential fits (dashed lines) are shown in the graph. Inset: A short scan at 1990 cm^{-1} showing the instrument-limited rise due to formation of product **F** on the ultrafast time scale.

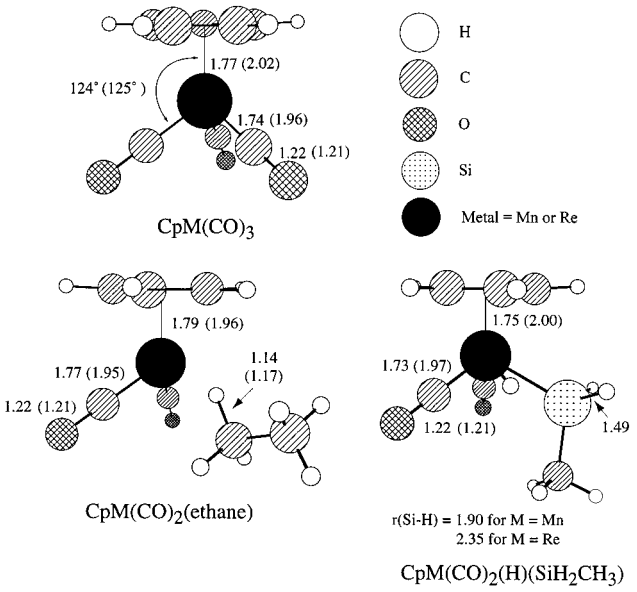

Figure 8. Geometries of the parent molecules, the ethane solvate, and the final product optimized at the MP2/lanl2dz level of theory. The bond lengths are in angstroms and angles in degrees. Parameters for the rhenium complexes are in parentheses.

0.2 μs exponential decay to a constant level. This finite absorbance is attributed to the CO stretch of $CpRe(^{13}CO)(^{12}CO)(H)(SiEt_3)$, estimated to be at 1892 cm^{-1}, the kinetics of which should be similar to those of the product.[37] The alkyl solvate **G**, therefore, displays a slightly longer decay time than the rise time of **F**. Similar to the treatment performed in the $CpMn(CO)_3/Et_3SiH$ system, the relative probability of the initial solvation through the ethyl group and the Si−H bond is estimated to be 75% and 25%, respectively. Assuming that transition-state theory is applicable, the measured rise time of the product gives an estimate of the free energy of the reaction barrier to be $\Delta G^{\ddagger} = 10.41 \pm 0.02$ kcal/mol (eq 5). Thus, the apparent rate-determining step is shown to be the dissociative rearrangement of the initial alkyl solvate, similar to the manganese reaction.

C. Ab Initio Calculation Results. Geometry Optimization. Figure 8 shows the geometries of the parent molecules η^5-$CpM(CO)_3$,[44] the dicarbonylmetal complexes solvated by an ethane molecule η^5-$CpM(CO)_2$ (ethane), and the final products η^5-$CpM(CO)_2(H)(SiH_2CH_3)$, all optimized at the MP2/lanl2dz level of theory. As displayed in Table 1, the metal−Cp and metal−CO distances for the parent molecules calculated at the MP2 level agree reasonably well with the experimental values, except for the slightly overestimated C−O bond lengths. Qualitatively, the metal−ligand distances should reflect the relative sizes of the manganese and the rhenium atoms. As displayed in Table 1, the rhenium complexes exhibit consistently a longer metal−ligand distance by ~0.17 Å over the manganese complexes, indicating a larger diameter for a complexed Re atom over a Mn atom.

For the ethane dicarbonyl complexes in Figure 8, the ethane molecule interacts with the metal center via one of its C−H bonds through an η^2 interaction. The bond lengths for the coupling C−H bond are 1.14 and 1.17 Å for the Mn and Re compounds, respectively. These calculated C−H bond lengths, compared to 1.10 Å for a typical C−H bond in a saturated alkane from the same level of calculation, show a significantly extended C−H bond (+0.07 Å) when complexed to the Re center but only slight (+0.04 Å) extension when coupled to the Mn complex. The more extended C−H bond in the Re case suggests that the Re atom interacts more strongly with a C−H bond, hence forming a more stable alkyl complex. Finally, the relative extent of the Si−H bond activation by the Mn and Re compounds is clearly demonstrated by the Si−H bond distances in the final products. The calculated Si−H bond lengths for the Mn and Re complexes are respectively 1.90 and 2.35 Å, compared to a typical silane Si−H bond length of 1.49 Å. Apparently, the degree of bond-breakage can be inferred from the product Si−H bond lengths. In the hydridosilyl manganese product, the Si−H bond is 0.41 Å longer than a Si−H bond in an isolated silane. The hydridosilyl rhenium product, on the other hand, exhibits a much longer distance (0.86 Å longer than an isolated Si−H bond) between the silicon and the hydrogen atoms, marking a completely broken Si−H bond.

Shown in Figure 9 are the geometries for the 16-e^- species η^5-$CpM(CO)_2$ in their singlet and triplet states. Despite the similarity of the structures, one notices a difference in the OC−M−CO angle. Due to the larger radius of the Re atom and, hence, reduced ligand−ligand repulsive interaction, the angle is 93.47° for the Re complex, compared to 95.11° for the Mn one or, when projected onto the Cp plane, 121° for the Re and 128° for the Mn species.

For both metal complexes, the geometries for the singlet species are quite different from the triplet ones; most notable are the positions of the M−CO bond relative to the molecular C_{2v} plane. For example, the angle between the M−CO bond and the molecular C_{2v} plane for the singlet state η^5-$CpMn(CO)_2$ is 64°, but it is 87° for the triplet state. In addition, the M−Cp and M−CO distances of the triplet species are longer than those of the singlet ones. Also, the CO bond lengths are shorter in the triplet states compared to those of the singlet states. Such a decrease in the metal−CO interaction in the triplet state has also been observed in Siegbahn's calculations of CpM(CO) (M = Co, Rh, and Ir).[45] Also shown in Table 1 are the DFT results for the 16-e^- species which are in general agreement with those

(44) The MacMolPlt package used for this graphical illustration was obtained from http://www.msg.ameslab.gov/GAMESS/Graphics/MacMolPlt.shtml.

(45) Siegbahn, P. E. M. *J. Am. Chem. Soc.* **1996**, *118*, 1487.

Table 1. Critical Bond Distances (Å) of the Important Structures for the Si−H Bond Activation Reactions Optimized at the MP2/lanl2dz Level of Theory[a]

compound	Cp−M	M−CO	C−O	M−H	M−Si(C)	Si−H (C−H)
η^5-CpMn(CO)$_3$	1.77 (1.77)[b]	1.74 (1.78)[b]	1.22 (1.16)[b]			
singlet η^5-CpMn(CO)$_2$	1.80 [1.86]	1.78 [1.79]	1.21 [1.19]			
triplet η^5-CpMn(CO)$_2$	1.84 [1.94]	1.82 [1.83]	1.19 [1.18]			
η^5-CpMn(CO)$_2$(H$_3$CCH$_3$)	1.79	1.77	1.22	1.77	2.73	1.14
η^5-CpMn(CO)$_2$(H)(SiH$_2$CH$_3$)	1.75	1.73	1.22	1.51	2.44	1.90
η^5-CpRe(CO)$_3$	2.02 (1.96)[c]	1.96 (1.90)[c]	1.21 (1.17)[c]			
singlet η^5-CpRe(CO)$_2$	1.94 [1.97]	1.95 [1.89]	1.22 [1.19]			
triplet η^5-CpRe(CO)$_2$	2.03 [2.04]	1.98 [1.91]	1.19 [1.19]			
η^5-CpRe(CO)$_2$(H$_3$CCH$_3$)	1.96	1.95	1.21	1.89	2.84	1.17
η^5-CpRe(CO)$_2$(H)(SiH$_2$CH$_3$)	2.00	1.97	1.21	1.69	2.57	2.35

[a] Numbers in parentheses are experimental values, and those in square brackets are from DFT calculations. [b] Fitzpatrick, P. J.; Le Page, Y.; Sedman, J.; Butler, I. S. *Inorg. Chem.* **1981**, *20*, 2852. [c] Fitzpatrick, P. J.; Le Page, Y.; Sedman, J.; Butler, I. S., *Acta Crystallogr., Sect. B* **1981**, *B37*, 1052.

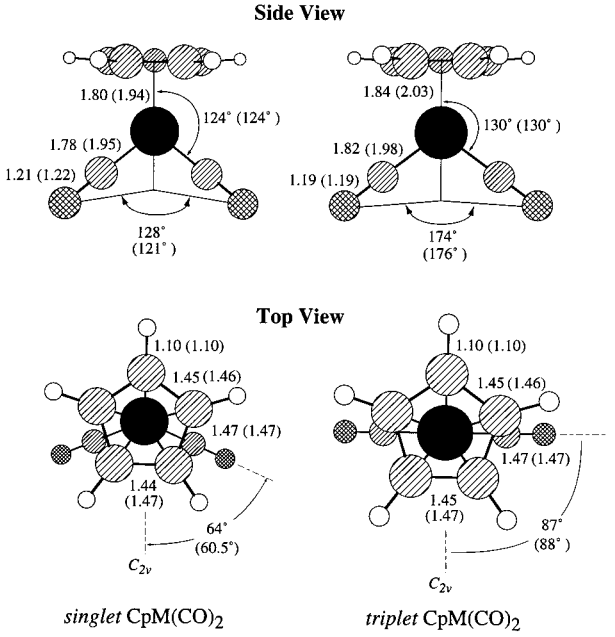

Figure 9. Side view and top view for the MP2/lanl2dz optimized geometries of the 16-e$^-$ species. The bond lengths are in angstroms and angles in degrees. Parameters for the rhenium complexes are in parentheses.

from the MP2 calculations. The DFT-calculated angle between the M−CO bond and the molecular C_{2v} plane for the singlet-state η^5-CpMn(CO)$_2$ is 63°, and it is 84° for the triplet state. Analogous parameters for the singlet and triplet rhenium complexes are 58° and 88°, respectively. The C−O bond lengths predicted by DFT methods, however, are consistently shorter than those predicted by MP2 methods. The Cp−Mn distance from DFT calculations is significantly longer than that from UMP2 methods (by ∼0.1 Å), perhaps due to the inadequacy of the UMP2 wave functions for describing high-spin species. These geometric parameters are summarized in Table 1. Several attempts to optimize η^3-CpMn(CO)$_2$, η^3-CpMn(CO)$_2$(CH$_4$), or η^3-CpMn(CO)$_2$(SiH$_4$) were unsuccessful, however, as an η^5-CpMn(CO)$_2$ configuration was invariably obtained, regardless of the initial guess.

Energy Calculations. The calculated metal−ligand interaction energies are listed in Table 2. After BSSE and ZPE corrections, the binding energies between the Mn complex and the CO ligand or the Si−H bond appear to be in good agreement with the experimental values. Compared to the Mn complex, the Re complex shows a binding energy to the CO ligand which is stronger by 5.81 kcal/mol. As a result, there is comparatively less excess energy available to the Re metal fragment after photolysis. Also, the hydridosilyl rhenium product is thermodynamically more stable than the manganese product by a marked 11.98 kcal/mol. In the case of an alkane ligand, it has been found experimentally[46] and theoretically[47] that the interaction energy between a transition metal and a series of chain alkanes may increase with alkane chain length. Consequently, in the present calculation, which uses ethane as the complexed solvent to model the solvation of η^5-CpM(CO)$_2$ through the ethyl group of Et$_3$SiH, the complexation energies obtained are likely to be underestimated. Nonetheless, the calculated binding energies of the ethane with Mn and Re complexes allow a qualitative understanding of the relative stability of η^5-CpMn(CO)$_2$ (alkane) and η^5-CpRe(CO)$_2$ (alkane). Our results show that an ethane molecule binds more strongly to the Re complex than to the Mn complex by about 3.5 kcal/mol. Similar stability for the η^5-CpRe(CO)$_2$L (L = *n*-heptane, Xe, and Kr) has also been reported in a recent paper by Sun et al.[48] Consequently, if the free-energy barrier of a dissociative rearrangement is dominated by the enthalpy of complexation, it would take longer for an η^5-CpRe(CO)$_2$(Et$_3$SiH) to rearrange dissociatively to allow interaction of a Si−H bond with the metal center, in comparison with the manganese system. Our experimental results show that it takes 6.8 μs for the rhenium compound to undergo such a rearrangement, whereas only 177 ns is required for the analogous process involving the manganese compound or, equivalently, a 2.16 kcal/mol difference in their free-energy barrier.

We next turn to the relative energies of the singlet and the triplet η^5-CpMn(CO)$_2$. The DFT results show a lower energy for the triplet η^5-CpMn(CO)$_2$ relative to the singlet (ΔE = 8.09 kcal/mol), in contrast to the MP2 results, which predict a lower-energy singlet state by 10.93 kcal/mol. These conflicting results are probably due to the near-degeneracy of the singlet and the triplet states. Similar inconsistent results from different calculation methods have also been reported in the literature.[45] For CpCo(CO), Siegbahn found that the MP2 method gave a singlet ground state, whereas other methods, including DFT/B3LYP and CASPT2, consistently yield a triplet ground state. To minimize the near-degeneracy effect, CAS MCSCF-PT2 calculations were performed at the DFT geometries; the results predict a ground triplet state for η^5-CpMn(CO)$_2$, 9.86 kcal/mol lower than the singlet state. Therefore, our calculations are in favor of a triplet ground state. For the rhenium complexes, analogous calculations consistently predict a singlet ground state

(46) (a) Ishikawa, Y.; Brown, C. E.; Hackett, P. A.; Rayner, D. M. *Chem. Phys. Lett.* **1988**, *150*, 506. (b) Brown, C. E.; Ishikawa, Y.; Hackett, P. A.; Rayner, D. M. *J. Am. Chem. Soc.* **1990**, *112*, 2530.

(47) Zaric, S.; Hall, M. B. *J. Phys. Chem. A* **1997**, *101*, 4646.

(48) Sun, X.-Z.; Grills, D. C.; Nikiforov, S. M.; Poliakoff, M.; George, M. W. *J. Am. Chem. Soc.* **1997**, *119*, 7521.

Table 2. Calculated MP2/lanl2dz Binding Energies (kcal/mol) for Singlet η^5-CpM(CO)$_2$L, M = Mn, Re[a]

	Mn			Re		
L	ZPE	ΔE	ΔE(BSSE)	ZPE	ΔE	ΔE(BSSE)
CO	−2.26[b]	95.55	51.76 (55)[c]	−2.75[b]	97.87	57.57
Et	0.21[d]	16.21	2.91 (10)[e]	0.21[d]	20.56	6.41
SiH_3CH_3	111.93[d]	53.83	22.92 (24.4)[e]	109.62[d]	71.88	34.90

[a] Experimental values are in parentheses. [b] Calculated using HF frequencies. [c] Angelici, R. J.; Loewen, W. *Inorg. Chem.* **1967**, *6*, 682. [d] Calculated using MP2 frequencies. [e] Burkey, T. J. *J. Am. Chem. Soc.* **1990**, *112*, 8329.

Table 3. Comparison of the Energy Difference, $\Delta E = E$(singlet) − E(triplet) (kcal/mol), between the Singlet and Triplet η^5-CpM(CO)$_2$ Calculated Using Different Methods

	Mn	Re
MP2[a]	−10.93	−5.63
DFT[b]	8.09	−5.62
CASSCF−PT2[b]	9.86	−7.88

[a] Calculated at the MP2/lanl2dz optimized geometry. [b] Calculated at the B3LYP/lanl2dz optimized geometry.

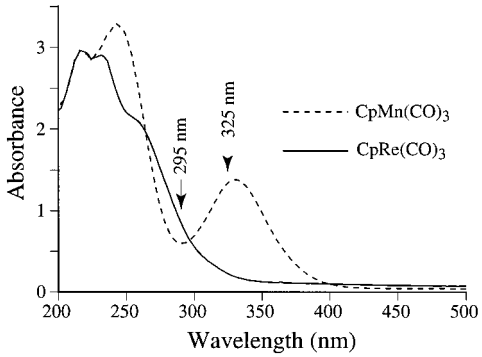

Figure 10. UV/vis spectra of the CpMn(CO)$_3$ and CpRe(CO)$_3$ in neat triethylsilane taken under experimental condition. Excitation wavelengths are indicated by arrows.

for η^5-CpRe(CO)$_2$. These results are summarized in Table 3. Finally, numerical CO stretching frequencies at DFT level were calculated for the singlet η^5-CpMn(CO)$_2$ (methane) (1889 and 1946 cm^{-1}) and for the triplet η^5-CpMn(CO)$_2$ (1870 and 1967 cm^{-1}). These results will be used in the assignment of **C** in the next section.[49]

IV. Discussion

A. Activation of the Silicon−Hydrogen Bond of Et_3SiH by CpMn(CO)$_3$. Effects of Excitation Wavelength. In the case of 295-nm excitation (paper I), the parent molecule η^5-CpMn(CO)$_3$ loses one CO ligand to produce two dicarbonyls (designated as **D*** and **C** in Figure 12); the former is quickly solvated to give **D**. The intermediate **C** then converts to form **D** on a time scale of 90 ps, or to **B** in ∼71 ps. The branching ratio in generating these two intermediates at this excitation wavelength, calculated in paper I from the kinetic trace of **D**, is approximately 1:1. Since this pump energy resides in the trough of two electronic states (see Figure 10), it is conceivable that **D*** and **C** may be related to the two electronically excited states. To examine how the excited states affect the reaction mechanism, we changed the excitation wavelength to the lower-energy band at 325 nm in the current study. Compared to excitation at 295 nm, the 325-nm excitation light injects less energy to the chemical system and samples different regions of the excited potential energy surface (PES). As a result, it may lead to dissociation channels that have different product energy distribution. Indeed, the kinetics of **C** and **D** following 325-nm excitation show little, if any, excess vibrational energy. This is to be compared with results from 295-nm excitation, which indicate that ∼23 ps is required to dissipate excess vibrational energy. For clarity, the kinetic traces of **D** recorded at the two pump energies are reproduced in Figure 11. Accessing a different part of the excited PES also changes the branching ratio from **A** → **D*** → **D**:**A** → **C** → **D** ≈ 1:1 (295-nm excitation) to 1:3 (325-nm excitation). This may imply that the lower-energy band at ∼330 nm correlates with the dissociation channel that leads to **C** and the higher-energy band to **D**.

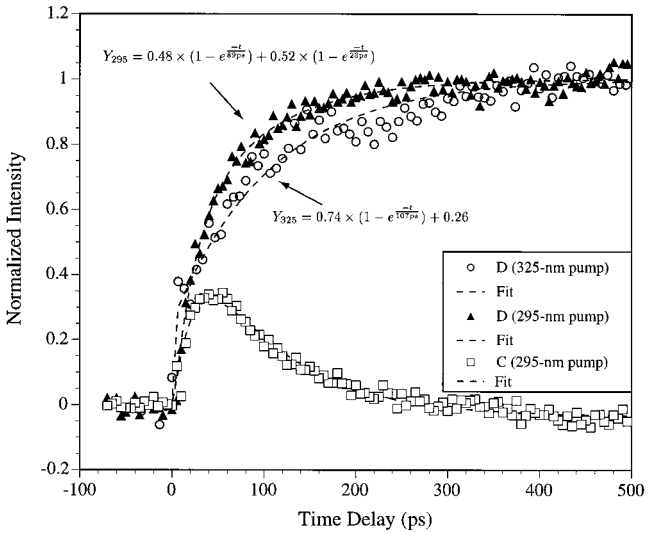

Figure 11. Ultrafast kinetic traces of **D** (▲), **C** (□) following 295-nm excitation, and **D** (○) following 325-nm excitation. Also shown are the functions Y_{295} and Y_{325} that are used to model the two normalized traces of **D**. Corresponding fits are shown as dashed lines. Clearly, the relative intensity of **C** to **D** is lower when excited at 295 nm compared to that at 325-nm excitation in Figure 2. This wavelength dependence can be quantified by comparing the fitting coefficients of Y_{295} and Y_{325}. See text for details.

Nature of the Intermediate C. In paper I, two possible candidates for the observed transient intermediate **C** were proposed: a ring-slipped η^3-CpMn(CO)$_2$ or η^5-CpMn(CO)$_2$ in another electronic state, presumably a triplet state. The η^3-CpMn(CO)$_2$ species,[50] however, has only 14 valence electrons for the Mn—a first-row transition metal—severely violating the 18-e$^-$ rule. Our theoretical modelings also support the energetic instability of η^3 complexes. **C** is therefore unlikely to be a ring-slipped 14-e$^-$ species. Another possible assignment for **C** is that it is a dicarbonyl in the triplet ground state. There have been precedents for 16-e$^-$ organometallics having a triplet ground state,[51−54] the geometry of which may differ from that

(49) The frequencies for a triplet dicarbonyl were determined on the η^5-CpMn(CO)$_2$ instead of η^5-CpMn(CO)$_2$ (alkane) because it is only weakly solvated by alkanes, to be discussed in the next section.

(50) (a) O'Connor, J. M.; Casey, C. P. *Chem. Rev.* **1987**, *87*, 307. (b) Lees, A. J.; Purwoko, A. A. *Coord. Chem. Rev.* **1994**, *132*, 155. (c) Basolo, F. *New J. Chem.* **1994**, *18*, 19.

(51) Bengali, A. A.; Bergman, R. G.; Moore, C. B. *J. Am. Chem. Soc.* **1995**, *117*, 3879.

of the singlet state to allow a different ligand vibrational frequency.[55] Our calculations suggest a triplet ground state for η^5-CpMn(CO)$_2$. We next compare the theoretical CO stretching frequencies to the experimental results. Recent developments in ab initio methods have shown promising results in identifying organometallic species through frequency calculations.[56] The DFT calculations for the triplet dicarbonyl show a $+21$-cm^{-1} shift of the higher-energy CO band and a -19-cm^{-1} shift of the lower-energy band of the solvated singlet dicarbonyl, compatible with experimental observation of frequency shifts of **C** relative to **D**. Therefore, it seems reasonable to attribute **C** to a triplet η^5-CpMn(CO)$_2$.

Solvation of the Triplet and Singlet Manganese Dicarbonyls. In the context of **C** being a triplet-state η^5-CpMn(CO)$_2$, we next discuss the interaction of **C** and the solvent. Unlike the singlet 16-e$^-$ species, which can be solvated readily by alkanes and rare-gas atoms (Kr, Xe), it has been suggested theoretically that transition metals in their triplet state interact only weakly with these solvents.[57] This conclusion has been used to explain the high reactivity of triplet η^5-CpCo(CO) toward a free CO in liquefied rare-gas solution or in alkane solution.[51] In that case, the incoming CO ligand does not require much activation energy to displace an alkane or rare-gas molecule which couples weakly to the metal center of η^5-CpCo(CO). Triplet-to-singlet intersystem crossing in chemical systems such as triplet η^5-CpCo(CO) or triplet η^5-CpMn(CO)$_2$ is further complicated by the fact that the complex of interest is always under the influence of solvent molecules in a liquid environment. It was found by Dougherty and Heilweil that triplet η^5-CpCo(CO) reacts very quickly (<vibrational cooling time) with the strongly binding ligand 1-hexene to form presumably a singlet π-complex, in which a 1-hexene molecule complexes to the Co metal through its C═C double bond.[43] This is to be compared with the lifetime (∼milliseconds) of triplet η^5-CpCo(CO) in weakly binding solvents such as Kr and Xe.[51] Hence, the surrounding solvent molecules, especially those interacting strongly with the metal center, need to be considered in describing the reaction coordinate for spin-crossover and solvent exchange. In other words, the interconversion from triplet **C** to singlet **D** should probably be considered as a concerted spin-crossover/solvation process.

With this picture in mind, the solvation of the initially photogenerated triplet and singlet dicarbonyls can be described as follows. Probably due to steric hindrance and statistical favor of the ethyl groups over the Si−H bond, the nascent singlet η^5-CpMn(CO)$_2$ is preferentially solvated via the ethyl moiety of Et$_3$SiH to form **D**. The solvation of the triplet dicarbonyl, however, may be quite different. Assuming that a triplet η^5-CpMn(CO)$_2$ interacts initially with the ethyl moiety of an Et$_3$SiH molecule, the interaction between the alkyl group and a triplet Mn is so weak that the surrounding solvent molecules have sufficient thermal energy to easily reorient or displace the interacting Et$_3$SiH, until the triplet Mn encounters a strongly coupling Si−H site. This process is expected to be on the order of a few picoseconds, the time scale for typical solvent motions. It would thus appear that a triplet transition metal complex is preferentially solvated by the more strongly coupling sites of a solvent molecule. Similarly a preferential solvation has also been observed in Heilweil's experiments on CpCo(CO) in neat 1-hexene, where one would expect to see solvation of CpCo(CO) through both the alkyl chain and the C═C bond of 1-hexene. The only product observed, however, was the strongly bound π-complex. Our data show that the product kinetics exhibit only one exponential rise on the ultrafast time scale, which is perhaps due to the preferential initial solvation of the singlet η^5-CpMn(CO)$_2$ via the ethyl group and the triplet η^5-CpMn(CO)$_2$ through the stronger-binding Si−H bond of the solvent molecule.

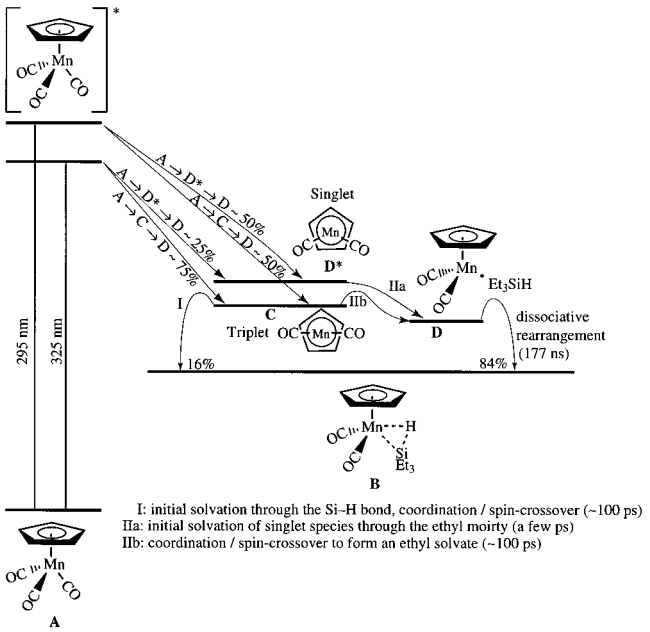

Figure 12. Proposed reaction mechanism for the silicon−hydrogen bond activation by CpMn(CO)$_3$ covering the ultrafast dynamics to nanosecond kinetics. The nascent singlet η^5-CpMn(CO)$_2$, denoted **D***, is also shown for the purpose of discussion. See text for details.

The Reaction Mechanism. In light of the above discussion, the photochemical Si−H bond activation reaction of η^5-CpMn(CO)$_3$ in neat Et$_3$SiH under the ambient conditions is summarized in Figure 12. We found that there are two excited states involved in the experimentally accessible region. The higher-energy UV band is correlated with the generation of the dicarbonyl η^5-CpMn(CO)$_2$(**D***) in its electronic singlet manifold, while the lower-energy band is correlated to the triplet η^5-CpMn(CO)$_2$ (**C**). Following the previous discussion on the preferential solvation of **D*** through the ethyl moiety and the fact that 84% of the total product comes from **D**, the branching ratio for **A** → **D*** to **A** → **C** can be calculated to be 42%:58% at 295-nm excitation. The initial solvation of these two intermediates via the Si−H bond or the ethyl moiety of the solvent partitions the reaction into two pathways with a branching ratio close to 1:5.3 (16% through the Si−H bond and 84% through the ethyl group). Solvation of **C** via the Si−H bond leads to the final product **B** on a time scale of ∼100 ps, possibly through a concerted coordination/spin-crossover process. Solvation of **D*** through the ethyl group of the solvent molecule results in **D**, whose population is augmented by interconversion from the triplet **C** on a similar time scale of ∼100 ps. Finally, the ethyl solvate reacts to form the final product **B** through a dissociative

(52) Abugideiri, F.; Keogh, D. W.; Poli, R. *J. Chem. Soc., Chem. Commun.* **1994** 2317.
(53) Detrich, J. L.; Reinaud, O. M.; Rheingold, A. L.; Theopold, K. H. *J. Am. Chem. Soc.* **1995**, *117*, 11745.
(54) Poliakoff, M.; Weitz, E. *Acc. Chem. Res.* **1987**, *20* 408.
(55) (a) Rawlins, K.A.; Lees, A. J. *Inorg. Chem.* **1989**, *28*, 2154. (b) Servaas, P. C.; van Dijk, H. K.; Snoeck, T. L.; Stuhkens, D. J.; Oskam, A. *Inorg. Chem.* **1985**, *24*, 4494.
(56) (a) Jonas, V.; Thiel, W. *J. Chem. Phys.* **1996**, *105*, 3636. (b) Zaric, S.; Couty, M.; Hall, M. B. *J. Am. Chem. Soc.* **1997**, *119*, 2885. (c) Zaric, S.; Hall, M. B. *J. Phys. Chem.* **1998**, *102*, 1963.
(57) (a) Blomberg, M. R. A.; Siegbahn, P. E. M.; Svensson, M. *J. Am. Chem. Soc.* **1992**, *114*, 6095. (b) Siegbahn, P. E. M.; Svensson, M. *J. Am. Chem. Soc.* **1994**, *116*, 10124. (c) Carroll, J. J.; Weisshaar, J. C.; Haug, K. L.; Blomberg, M. R. A.; Siegbahn, P. E. M.; Svensson, M. *J. Phys. Chem.* **1995**, *99*, 13955.

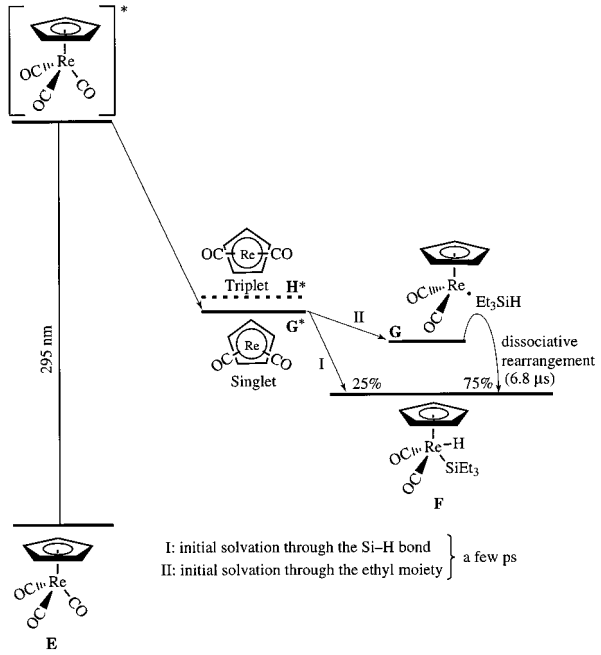

Figure 13. Proposed reaction mechanism for the silicon−hydrogen bond activation by $CpRe(CO)_3$ covering the ultrafast dynamics to microsecond kinetics. The nascent singlet and triplet η^5-$CpRe(CO)_2$, denoted **H*** and **G***, are also shown for the purpose of discussion. See text for details.

rearrangement on a time scale of ∼177 ns, corresponding to a barrier height of $\Delta G^{\ddagger} \approx 8.25$ kcal/mol.

B. Activation of the Silicon−Hydrogen Bond of Et_3SiH by $CpRe(CO)_3$. In comparison to the manganese compound, the photochemical reaction of η^5-$CpRe(CO)_3$ (**E**) with Et_3SiH is much simpler (see Figure 13). Photolysis of **E** results in a dicarbonyl species, η^5-$CpRe(CO)_2$ (**G***), in its singlet electronic ground state. Subsequent solvation of **G*** partitions the reaction into two courses to the formation of the final product. Interaction of **G*** with the Si−H bond of the solvent molecule leads directly to the final product η^5-$CpRe(CO)_2(H)(SiEt_3)$ (**F**), with a time constant of ∼4.4 ps. Another pathway proceeds through solvation of **G*** via the ethyl group of the solvent to form η^5-$CpRe(CO)_2(Et_3SiH)$ (**G**) on a time scale of ∼2.5 ps and further reacts to form the final product **F**. The relative probability of (solvation through the ethyl moiety)/(solvation through the Si−H bond) for the rhenium complex is found to be approximately 3, compared to 5.3 for the manganese complex. The difference may be attributed to steric interaction from the ligands. The smaller radius of the Mn center may cause increased steric interaction between the ligands and the solvent molecule's ethyl group when solvation proceeds through the Si−H bond. Such steric hindrance is reduced when solvation occurs through the ethyl moiety. The larger diameter of the Re center makes it more accessible to chemically different sites of a solvent molecule, resulting in a branching ratio of approximately 3—the ratio of three ethyl groups to one Si−H bond in an Et_3SiH molecule.

V. Closing Remarks

Due to the very complicated dynamic processes in a liquid environment, photochemical reactions such as the bond-activation reactions studied here may span several orders of magnitude in time—from hundreds of femtosecond for dissociating a chemical bond to the time scale governed by a diffusional process or an energetic barrier. Combining the use of the femtosecond and nanosecond UV pump-IR probe spectroscopy, the elementary reaction steps including changes in molecular conformation and electronic multiplicity may be studied by monitoring the time evolution of the reactive intermediates. The nature of the intermediates whose lifetimes were too short for conventional spectroscopic characterization were studied using first-principle quantum chemical methods. Utilizing these powerful tools, it is also possible to assess the relative probability of *parallel, dynamically partitioned* reaction channels. We have investigated photochemical Si−H bond activation reaction by group VIIB, d^6 transition metal complexes η^5-$CpM(CO)_3$ (M = Mn, Re). The detailed reaction mechanisms are summarized in Figures 12 and 13.

Despite the fact that Mn and Re belong to the same group in the periodic table, we have shown in this paper that the reaction dynamics of η^5-$CpMn(CO)_3$ or η^5-$CpRe(CO)_3$ with Et_3SiH is very different on the ultrafast time scale and depends on the nature of electronic structure of the molecule in question. If more than one dissociation channel (excited state) is involved in the initial photolysis, as in the Mn case, which has two experimentally accessible UV bands, the reaction may dynamically partition into several parallel pathways leading to different transient intermediates. The nature of these transient species have been investigated using ab initio calculations. The calculation results provided strong evidence that photolysis of the parent η^5-$CpMn(CO)_3$ generates both singlet and triplet $CpMn(CO)_2$ species, which accounts for the experimental observations consistently. The correlation of these reaction pathways to the excited states was studied by examination of their branching ratios, which were determined from ultrafast kinetic traces of the intermediates, at different excitation wavelengths. In the case of Mn, the higher-energy band was found to associate with formation of singlet η^5-$CpMn(CO)_2$, while the lower-energy band was found to associate with that of triplet η^5-$CpMn(CO)_2$. Interactions of solvent molecules with the singlet and triplet Mn complexes were also discussed.

The metal dicarbonyls η^5-$CpMn(CO)_2$ and η^5-$CpRe(CO)_2$ resulting from UV photolysis of a CO ligand were found to be solvated by a solvent molecule in a few picoseconds. From this point on, both metal complexes share a common reaction pattern, in which solvation through chemically different sites of a solvent molecule further partitions the reaction into two routes. The final product could form on the ultrafast regime when the coordinatively unsaturated 16-e^- metal complex interacted with the Si−H bond of the solvent molecule. On longer time scales, both reactions (Mn and Re) were shown to proceed through a kinetically favored intermediate—a metal dicarbonyl solvated by the ethyl moiety of solvent molecule. The branching ratio for these solvation-partitioned reaction pathways, derived from the product kinetic traces taken at nano- or microsecond time scales, was argued to be governed by steric interaction. The apparent rate-determining step was found to originate from dissociative rearrangement from this ethyl solvate to the thermodynamically more stable hydridosilyl product. The associated free-energy barriers were also determined and were in excellent agreement with results from previous low-temperature studies (for Mn).

Through detailed mechanistic study, we were able to experimentally determine the Si−H bond-breaking step. The time scale for such a process in a liquid environment was, for the first time, measured to be 4.4 ps. The result allows an upper bound for the time scale of the Si−H bond-activation step, confirming ab initio theoretical predictions.[58] This is in sharp

(58) (a) Koga, N.; Morokuma, K. *J. Am. Chem. Soc.* **1993**, *115*, 6883. (b) Musaev, D. G.; Morokuma, K. *J. Am. Chem. Soc.* **1995**, *117*, 799.

contrast to the analogous C−H bond-cleaving process, which takes approximately 230 ns.[4] In this case, the 8.3 kcal/mol energy barrier corresponding to cleaving an alkane C−H bond has been attributed to poor spatial overlap and energy match of the molecular orbitals between an alkane C−H bond and a transition metal center; the hydrogen atom and an alkyl group have to separate before forming chemical bonds with the metal center.[58] Extension of the current work, including a close interplay between experiment and theory, to other transition metals reacting with different chemical bonds is expected to provide a better understanding about the chemistry of bond-cleavage reactions.

Acknowledgment. This work was supported by a grant from the National Science Foundation. We thank R. G. Bergman for many helpful discussions; K. Morokuma for suggestions on the ab initio calculations; C. B. Moore for the use of the static FTIR spectrometer; and J. Yeston and P. J. Alaimo for assistance with handling of the samples.

VI. Appendix

In the ultrafast experiment of η^5-CpRe(CO)$_3$/Et$_3$SiH, several events that occur concurrently on the ~100-ps time scale have complicated the transient spectra in the frequency region from 1990 to 2030 cm^{-1}. These events include the recovery of the parent η^5-CpRe(^{12}CO)$_3$ bleach due to reequilibration of the vibrational population, bleach recovery of η^5-CpRe(^{12}CO)$_2$-(^{13}CO), and the formation of the product η^5-CpRe(CO)$_2$(H)-(SiEt$_3$). Summarized below are these processes and their associated frequencies:

1990 cm^{-1}: product formation,
vibrational relaxation of $^{13}v = 2$

2004 cm^{-1}: vibrational relaxation of $^{13}v = 1$

2015 cm^{-1}: bleach recovery of $^{13}v = 0$,
vibrational relaxation of $^{12}v = 1$

2030 cm^{-1}: bleach recovery of $^{12}v = 0$

where superscripts 12 and 13 refer respectively to the parent molecule η^5-CpRe(^{12}CO)$_3$ and the naturally abundant ^{13}CO monosubstituted η^5-CpRe(^{13}CO)(^{12}CO)$_2$. To deconvolve the dynamics of individual events out of the complicated spectra, we first consider the population of the *i*th vibrational state of η^5-CpRe(^{13}CO)(^{12}CO)$_2$. Assuming that the relaxation rate of the *i* state to the $i-1$ state is proportional to the population n_i, and that n_i is replenished only by relaxation from the $i+1$ state, we can write the coupled rate equations for vibrational states $i = 0$, 1, and 2 as

$$\frac{\mathrm{d}(^{13}n_i)}{\mathrm{d}t} = -^{13}k_{i,i-1}\,^{13}n_i + ^{13}k_{i+1,i}\,^{13}n_{i+1} \tag{6}$$

where $k_{i,j}$ s are the rate constants for the transition from *i* state to *j* state. Similarly, the population dynamics for CO vibrational states $i = 0$ and 1 of η^5-CpRe(^{12}CO)$_3$ can be expressed as

$$\frac{\mathrm{d}(^{12}n_0)}{\mathrm{d}t} = ^{12}k_{1,0}\,^{12}n_1 \tag{7}$$

$$\frac{\mathrm{d}(^{12}n_1)}{\mathrm{d}t} = -^{12}k_{1,0}\,^{12}n_1 \tag{8}$$

Finally, the formation of the final product at 1990 cm^{-1} is assumed to be represented by a single exponential,

$$I_{\mathrm{product}} = C_{\mathrm{product}}(1 - \mathrm{e}^{-t/\tau_{\mathrm{product}}}) \tag{9}$$

We further assume that the IR absorbance of state *i*, denoted by I_i, is proportional to its population n_i. The observed kinetic traces can then be fit to this model by solving the coupled differential equations (eqs 6−8) numerically and collecting terms contributing to the relevant frequencies. The optimized parameters are as follows: $^{13}I^0_3 = 0.29 \pm 0.15$, $^{13}I^0_2 = 1.30 \pm 0.015$, $^{13}I^0_1 = 0.92 \pm 0.070$, $^{13}I^0_0 = -3.24 \pm 0.16$, $^{13}k_{3,2} = 0.083 \pm 0.0036$ ps^{-1}, $^{13}k_{2,1} = 0.088 \pm 0.0076$ ps^{-1}, $^{13}k_{1,0} = 0.088 \pm 0.015$ ps^{-1}, $^{12}k_{1,0} = 0.032 \pm 0.0025$ ps^{-1}, and $\tau_{\mathrm{product}} = 4.35 \pm 2.6$ ps. The deconvolved kinetic traces are displayed in Figure 6 and explained in the figure caption. Note that the intensities at $t = 0$ of state *i*, denoted by I^0_i, do *not* reflect the initial population on each vibrational state, since we do not have a priori knowledge of the extinction coefficient for each vibrational state.

JA980692F